Microstructure, mechanical properties, and adhesion in IN625 air plasma sprayed coatings

Thomas Gnaeupel-Herold [a,*], Henry J. Prask [a], John Barker [a], Frank S. Biancaniello [b], Rodney D. Jiggetts [b], Jiri Matejicek [c]

[a] *National Institute of Standards and Technology, Center for Neutron Research, 100 Bureau Dr., Gaithersburg, MD 20899, USA*
[b] *National Institute of Standards and Technology, Metallurgy Division, 100 Bureau Dr., Gaithersburg, MD 20899, USA*
[c] *Institute of Plasma Physics, Za Slovankou 3, 18221 Praha, Czech Republic*

Abstract

The effects of feed stock particle size on the microstructure and the mechanical properties of IN625 air plasma sprayed coatings were investigated. It was found that the porosity increases with the particles size while the oxide content rises with decreasing particle size. Because of the lower velocity of large particles, these produce weakly bonded splats resulting in coatings with low elastic modulus, low residual stresses, small oxide content, and low hardness. The porosity is high and it is largely comprised of surface connected pores. Small particles produce splats that are bonded through oxide layers. Due to higher particle speed the porosity and the fraction of connected pores are low. The small porosity produces a relatively large value of Young's modulus and high residual stresses. The hardness increases as the porosity decreases and the oxide content increases. The coating adhesion exhibits a maximum at intermediate particle sizes. This is caused by the limiting effect of the oxide content for small particles and the limiting effect of low particle velocities for large particles.
© 2005 Elsevier B.V. All rights reserved.

Keywords: Particle size; Mechanical properties; Plasma sprayed coating; Neutron diffraction

1. Introduction

Thermal spray deposits of nickel-based alloys are used in numerous applications that involve protection against wear and corrosion, restoration layers for machine parts, or bond coats for thermal barrier coatings [1]. The successful use of the coatings depends to a large extent on its mechanical properties and on the adhesion to the substrate, both of which are closely linked to the coating microstructure. Numerous studies in recent years have investigated these inter-correlations. For example, it was found that a large degree of control over porosity, Young's modulus, hardness, and residual stresses can be achieved by a deposition within specific ranges of particle kinetic energies [2,3]. The observed correlation between mechanical properties and porosity has also received a great deal of attention elsewhere [4–8]. Following these investigations, the porosity can be classified into distinctive groups of pores: oblate, oriented pores with high aspect ratios, and volumetric pores.

The oblate pores originate from incomplete contact of adjacent splats due to insufficient wetting. These voids are generally flat with high aspect ratios, and their dominant orientation is parallel to the substrate. Vertically oriented voids are present between horizontally (i.e. parallel to the substrate surface) adjacent splats. The oblate pores are the largest contributor to the inner surface area but they represent only a small fraction of the total porosity [4]. Due to their high aspect ratios these voids have a major effect on the elastic constants of the coatings because they effectively decrease the cross-section area of the coating [4,7,9,10]. Volumetric or globular pores exist because of trapped gases and due to incomplete filling of surface pits and gaps left by solidified splats. In one study, it was found that their contribution to the inner surface area is small but they represent up 30% of the total porosity [4]. The pore aspect ratio is small, and usually there is no preferred orientation of such pores. In small volume fractions, globular pores cause an approximately linear decrease of Young's modulus [11]. Depending on the spray conditions, some fraction of the pores is surface-connected. To our knowledge, the effect of a network pore structure on elastic properties has not been investigated yet but such a structure is likely to further reduce the elastic modulus. Factors such as particle speed and particle temperature have a strong influence on all aspects of the porosity [3].

---

* Corresponding author.

Residual stress in coatings is an important mechanical property because it has an influence on the tendency of the coating to de-bond from the substrate [3,6–8,12–17]. The sources of residual stresses in the coatings are the quenching of the molten particles upon impact and the differences between the coefficients of thermal expansion of coating and substrate. The residual stresses are indirectly affected by the pore structure because stresses depend on the elastic modulus as well as strain. The strains are mainly determined by the thermal conditions during the deposition process.

The adhesion of the coating to the substrate is assumed to be created by a mechanical interlock between the substrate surface and the first coating layer [18–20]. Thus, a certain degree of surface roughness – usually created by grit blasting – is necessary to achieve good results. Further contributions to adhesive strength of metallic coatings are metallurgical bonds that are created when a re-melting of the surface under solidifying splats occurs [2,19].

Another important feature for metallic deposits that are sprayed under atmospheric conditions is oxidation [21]. Oxides are usually concentrated on the splat surfaces. Their main effect is a strength increase of the coating as seen in large strain hardening exponents and a hardness increase [2]. With respect to general coating performance the general effect of increased oxide contents is seen as detrimental as this type of hardening behavior often leads to a loss in ductility.

In the following, we will discuss results from measurements covering the aforementioned topics: (1) the correlations between feed stock particle size and coating microstructure and (2) the mechanical properties, specifically elastic modulus, hardness, residual stresses, and adhesion. Results regarding the adhesion of NiCrAlY coatings will also be presented.

2. Experimental procedure

2.1. Sample preparation

The coatings were prepared by atmospheric plasma spraying at the thermal spray facility of the NIST Metallurgy Division. The substrates were low carbon steel slabs of dimensions 2.9 mm (t) × 29.5 mm (w) × 120 mm (l) with 20 grit Al_2O_3 grit-blasted surfaces ($R_a = 5 \mu m$). The substrates were pre-heated by two passes with the spray torch. The IN625 feed stock powder was produced by gas-atomization at the NIST Metallurgy Division. The particle size distributions were achieved by sieving. The details are listed in Tables 1 and 2.

The adhesion of NiCrAlY coatings was also investigated for which commercially available feed stock powders were used. Its composition is listed in Table 3.

The particle size range is −106 to +45 μm. The substrate material was the same as for the IN625 coatings but had three surface treatments: grit blasting, glass bead blasting, and HCl etching of the as-received steel slab surface. These were employed to investigate the effects of the surface condition on residual stresses and adhesive strength.

Table 1
Size distributions of the feedstock powders used

Cut	Particle size range (μm)	Coating thickness (mm) sample 1/sample 2/sample3
Fine	−30 to +25	0.36/0.40/0.44
Medium	−63 to +53	0.52/0.40/0.32
Coarse	−125 to +106	0.65/0.80/0.44
Mixed	−200 to +5	0.70/0.46/0.50

The uncertainty for the coating thickness is ±0.1 mm. Each cut was sprayed on three substrates so that a total of 12 samples were measured. The particle size range is given in standard notation for characterizing feed stock powders (first value is the upper limit, the second value is the lower limit).

Table 2
Composition of IN625 in wt.%

Cr	21.5
Mo	9.0
Nb	3.6
Ti	0.2
Al	0.2
Fe	4.0
Ni	61.5

2.2. Neutron diffraction

The neutron diffraction measurements were done using the residual stress diffractometer (BT8) at the NIST Center for Neutron Research, Gaithersburg, MD, U.S.A. The technique is explained in detail by Kesler et al. [3]. The coating thickness was found to be somewhat non-uniform because of the large surface roughness of the outer surface. The thickness measurements were done using a caliper on several locations on the coatings. The average values were from 0.4 up to 0.7 mm with an uncertainty of 0.1 mm whereas neutron beams usually have sizes of 0.5 mm or larger. Fig. 1 shows how the neutron measurement is done.

Measurements were done on three specimens for each coating with a total of nine locations for each specimen. The required unstressed d-spacing d_0 was obtained by using the mechanical boundary condition for the stress perpendicular to the surface at the surface $\sigma_{zz} = 0$. Assuming a uniform in-plane stress $\sigma_{xx} = \sigma_{yy}$, it allows the calculation of d_0 from d-spacings measured in the in-plane direction and in the perpendicular direction as explained in Ref. [22]. The presence of oxides is disregarded.

2.3. Elastic modulus

Once the strains are obtained, the specific elastic constants for each coating are needed to calculate the stress. These measurements were done both with free-standing (de-bonded) coatings

Table 3
Composition of NiCrAlY in wt.%

Cr	30.0
Al	10.0
Y	1.0
Ni	Balance
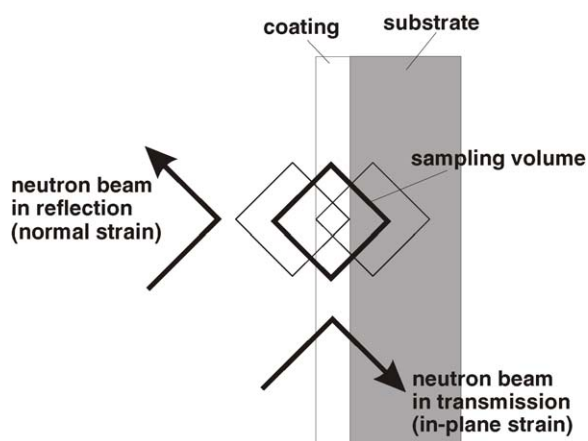
Fig. 1. Schematic of the neutron diffraction stress measurements on coatings. The size of the sampling volume was $2\,mm \times 2\,mm \times 7\,mm$. In each of the two orientations, the sample was moved through the beam in small steps and a diffraction peak was measured. The sampling volume with the bold outline indicates the center position from which the *d*-spacing was used to calculate the stresses.

and with coatings still bonded on the substrate composites using a four-point bending apparatus. The bending experiments were done according to the following procedure. Free-standing coatings were obtained by trimming off the rounded edges from the coating and applying a razor blade to remove the coating from the substrate. Four-point bending was performed both with the interface side of the coating in tension (outward bending) and in compression (inward bending). The in situ diffraction bending tests were done with the coating attached and in tension; the substrate modulus was determined from a bending test on a substrate strip without coating.

2.4. Porosity

The porosity was determined using two methods: small angle neutron scattering for the closed porosity and image analysis for the total porosity. The surface connected porosity was obtained from the difference of the two values.

For the image analysis, a dye-contrast method was used in which the coatings were immersed in a dye to fill the open and connected pores followed by gentle polishing. This was done for the cross-section at both ends of the coated strips. Optical image analysis was then used to determine the area percentage of dye filled regions for determining the porosity. It is assumed that the polishing does not reveal any additional pores that are not filled with dye. This procedure was performed for the top and bottom (beginning and end of spray pass) of each specimen with two specimens for each particle cut.

The closed porosity was determined with small angle neutron scattering at the perfect-crystal diffractometer (PCD) for ultra-high resolution small-angle neutron scattering (USANS) at the NIST Center for Neutron Research. First, the specimens were immersed in deuterium oxide (D_2O) under vacuum to enable better pore penetration. D_2O filled pores have almost the same scattering length density ($6.38 \times 10^{10}\,cm^{-2}$) as the surrounding solid material ($6.92 \times 10^{10}\,cm^{-2}$), thus effectively removing the

surface connected porosity contribution to the scattering signal (note: pores have a zero scattering length density). Note that the oxide volume fraction has to be included in the calculation of the scattering contrast. In order to obtain the connected porosity, the SANS result for the closed porosity was subtracted from the total porosity from image analysis.

We also investigated the direct SANS measurement of closed and connected porosity through dry and immersion measurements. This was not successful because of multiple scattering on the dry samples.

2.5. Oxide content

The weight fraction of oxides in the coatings was estimated using density measurements. The densities of IN625 feed stock powder and the density of the deposits were determined and, using the known densities of the oxides and the porosities as determined by image analysis, the oxide fraction was estimated from a linear mixing rule.

2.6. Hardness tests

Vickers hardness tests were conducted with 200 g load using a computer image analysis system. The indent dimensions were set manually. Indentation scans were performed both for the cross-section and for the plane section (600 grit polish for both on outer coating surface). The substrate hardness values are the average of 10 single measurements; the coating hardness values represent the average of approximately 30 single measurements in each direction.

2.7. Adhesion

The adhesion tests were done as tensile adhesion tests [23] on three square pieces for each sample with dimensions $10\,mm \times 10\,mm$. The ASTM standard [24] was used as guidance. Each piece was glued with a high strength adhesive bonding agent between two cylindrical tensile adapters. The adapters were then subjected to a tensile load and the force was recorded at which the coating de-bonded. The adhesive strength of the bonding agent was not measured; however, the bonding strength of the agent was specified to be >80 MPa, well above the adhesions strengths found. All failures occurred at the interface with no signs of contamination from the bonding agent.

3. Results and discussion

3.1. Microstructure

The optical inspection of the coatings in Fig. 2 showed that the characteristic features of inhomogeneity scaled well with the particle size of the feed stock powder. Individual splats, contact areas and pores are clearly identifiable, and their respective sizes scale with the particle size (Fig. 2). All coatings contain un-melted particles which are visible as spherical regions separated by a darker interface. Regions of this color were identified as oxides. The oxides are clearly aggregated around the
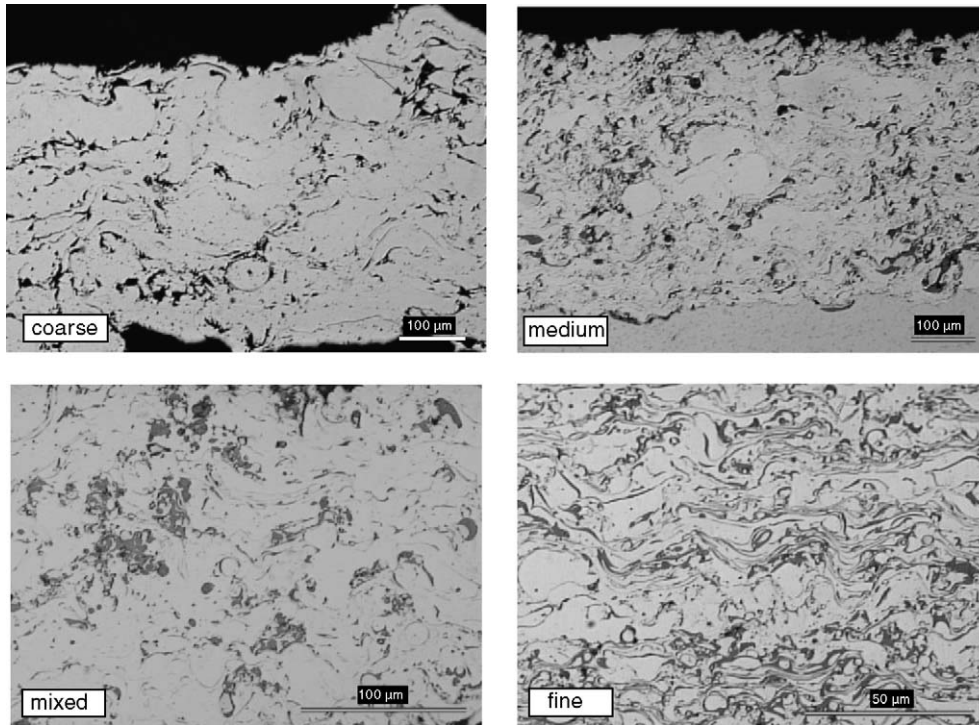
Fig. 2. Optical microscopy images for coatings sprayed with particle sized described in Table 1.

splat boundaries, thus suggesting substantial in-flight oxidation. Black regions are pores that were identified using dye penetration. The fine coatings contain regions of seemingly porosity free IN625 that are assumed to be the result of larger droplets formed by smaller droplets clumped together during flight. The splats and large pores visible in the coarse coating extend laterally up to 50% of the coating thickness. The largest contiguous vertical pore space (upper right corner of coarse coating in Fig. 2) is about 15% of the coating thickness. This is also approximately the thickness of large splats which show a low flattening ratio. This has been associated with low particle velocities and splat fragmentation [2], leading to poor contact between splats and splat separations.

For medium coatings, the size of these characteristic features is approximately half of the coarse coating (see Table 1 for particle size). The mixed and fine coatings do not show large pores but they have visible oxide layers surrounding the splats. The flattening ratios increase; both coatings appear denser and more compact than the coarse coating. Furthermore, in the fine coating oxide aggregation around splat boundaries is the dominant feature of the microstructure. The microstructure of the medium coating resembles that of the coarse coating with the feature size decreased proportionally. The mixed coating is characterized by a lower pore density than the coarse and medium coating while the splat boundaries are significantly less oxidized than the fine coating.

3.2. Porosity

The results of the quantitative investigation of the porosity is shown in Fig. 3. The SANS results for the total porosity were corrected for Cr_2O_3 oxide scattering. Generally, there is good

agreement between the porosity from image analysis and the porosity from SANS. Neither the SANS technique nor the image analysis used here provided information about shape and orientation of the pores. However, in the coarse coating the surface connected porosity represents >90% of the total porosity, thus making the pore structure essentially an open network of interconnected pores. For smaller particles the fraction of surface connected pores drops significantly.

3.3. Oxide content

The oxide addition was identified qualitatively by means of X-ray diffraction as Cr_2O_3. The strongest Cr_2O_3 reflection (1 1 0) found is shown in Fig. 4.
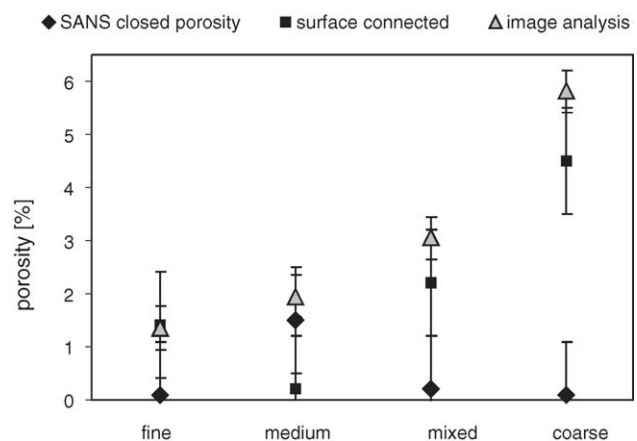
Fig. 3. Porosity values as determined by SANS (total and surface connected) and by image analysis.
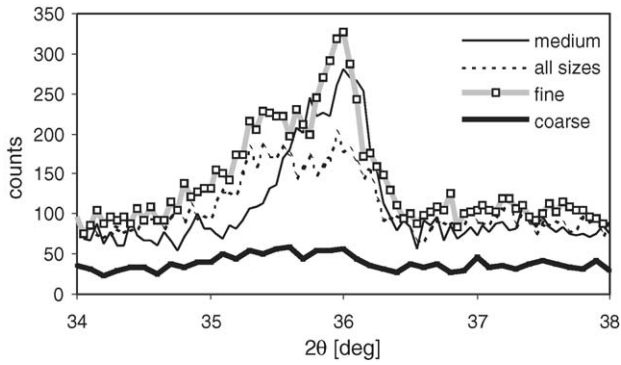
Fig. 4. The Cr_2O_3 (1 1 0) reflection measured by X-ray diffraction (Cu Kα radiation).

Based on the assumption that Cr_2O_3 is the only oxide present in the IN625 coatings the oxide content was estimated as shown in Table 4.

The estimate for the oxide fraction in Table 4 has to be considered as a lower limit because it is likely that also some NiO is also formed, although below the detection limit (≈5%) in the X-ray experiment. The strong increase of the oxide content is consistent with other findings that reported an exponential increase of the oxide content with decreasing particle size [21].

3.4. Deformation behavior and elastic modulus

When analyzing strains in coatings the lattice strain and the macroscopic strain have to be distinguished. Fig. 5 shows how the lattice strain depends on the applied strains. Fig. 6 shows the slopes of the strain response curves in Fig. 5 versus the porosity. The geometry for the in-plane measurement is shown in Fig. 1.

The average lattice strains in the in-plane direction in a porous structure are smaller than the applied strains. This suggests that a fraction of the applied strain is spent on opening or closing voids, depending on the sign of the applied strain (see Fig. 7). Unconnected pores are strained less than connected pores. There are also regions with poor interfacial contact or otherwise weakly bonded regions that have only a small strain response under applied strain, thus leading to low average lattice strains in the overall coating. A similar effect was observed in Ref. [2] on low porosity cold spray coatings with a Young's modulus comparable to that of higher porosity APS coatings. Incomplete contact between splats can be seen as enabling factor for connected porosity which, on the other hand, increases together with the

Table 4
Coating densities (corrected for porosity) and estimated oxide weight fractions

Coating	Density (g/cm^3)	Volume fraction Cr_2O_3 (%)
Fine	7.69	22.2
Medium	8.00	14.4
Mixed	7.94	12.5
Coarse	8.17	4.7
IN625 powder	8.26	

For Cr_2O_3 a density of 5.23 g/cm^3 was used. The uncertainty of the density measurement was 0.02 g/cm^3. The uncertainty of the oxide content is estimated to 4%.
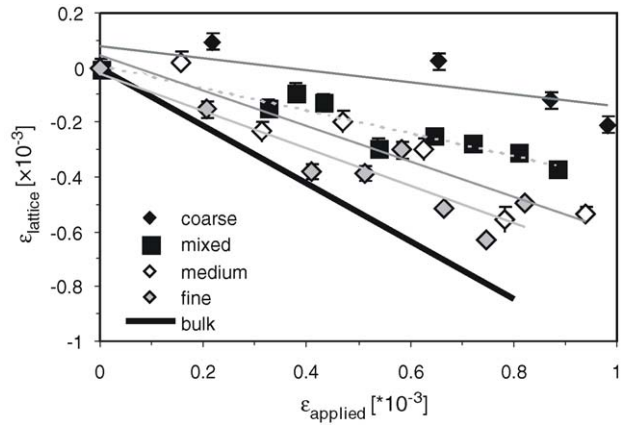
Fig. 5. Lattice strain (in-plane) vs. the average applied strain. The coatings were attached to their respective substrates and the average applied strains were calculated as the mean of the strain at the surface and the strain at the substrate/coating interface. The bulk value was calculated for the nickel (3 1 1) reflection (zero porosity) [25,26]. The straight lines represent the linear regression preformed.

total porosity as the particle size increases. The connected porosity is the dominant fraction of the total porosity (see Fig. 3) in the coarse particle coatings.

Additionally, local bending or rotations of small solid regions in the coating structure may occur, thus leading to highly non-uniform strain fields. It can also be expected that local yielding occurs at void tips or other regions of high stress concentration, thus – together with interfacial sliding as another possible mechanism – providing an inelastic contribution to the (elastic) lattice strains in Fig. 5. The common effect of these influences is the reduced response of average lattice strains as the porosity (and the connected porosity with it) increases as shown Fig. 6 where there is a three-fold increase of the strain response from 4.6% porosity (coarse) to 1.5% porosity (fine). This strong increase, according to continuum-mechanical models [9,11,27], points towards very large pore aspect ratios. This suggests that a large degree of connectivity between pores has a similar effect as an increased aspect ratio.

The results for Young's modulus are shown in Fig. 8.

In order for the lattice strain and the macroscopic strain to translate into the same stress the diffraction modulus must
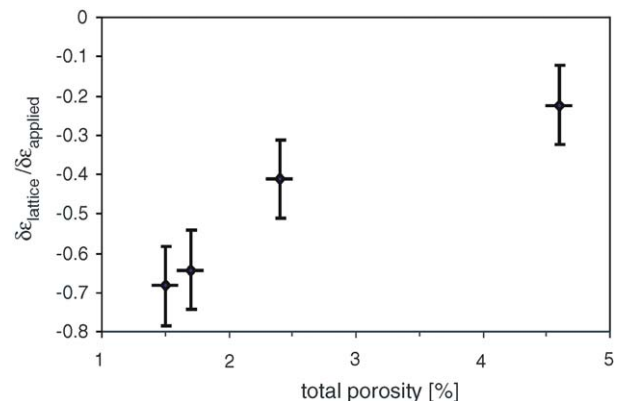
Fig. 6. Strain response (slope $\Delta\varepsilon_{lattice}/\Delta\varepsilon_{applied}$) of the lattice strains in Fig. 5 vs. porosity.

no applied strain | **with applied strain**

regions of high stress/strain   largely unstrained region
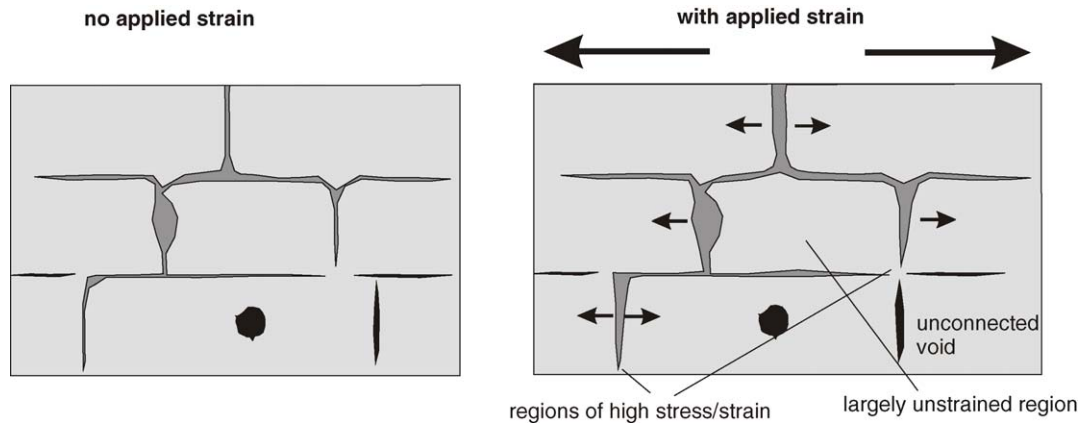
unconnected void

Fig. 7. Schematic of the deformation of a porous structure with interconnected voids. Light gray regions are splats, dark gray regions indicate connected pores, black regions are enclosed pores.

be substantially higher than the modulus from bending. The differences between bending in compression and bending in tension are within the experimental uncertainties. Similar to results reported elsewhere [2] the moduli of the free-standing coatings are only 20–50% of the bulk value ($E_{bulk} = 220$ GPa for nickel). Diffraction moduli are rarely reported in other works but their correct values are essential for diffraction stress measurements on coatings. For the fine, medium and mixed coating the experimental results are approximately equal to the diffraction value for the (3 1 1) reflection ($E_{(3\,1\,1)} = 214$ GPa, estimated for pure nickel and zero porosity). The low value for the coarse coating reflects the effects both of the high porosity, and the influence of inelastic processes as discussed on the strain response. It should be noted that the elastic modulus of IN625 is affected to a minor extent by the presence of Cr_2O_3 which has a modulus of 397 GPa, substantially higher than Ni [28]. Both phases form an elastic composite in which the metallic phase "sees" a matrix – the composite – that is elastically more stiff than the metallic phase alone. Thus, a diffraction measurement of the metallic phase yields a modulus that is $\approx$10% higher than a modulus measured in pure IN625 (lever rule). Therefore, both the lower porosity and the higher oxide content increase the elastic modulus in small particle coatings.

3.5. Hardness

Typical images of indents on cross-section surfaces are shown in Fig. 9. The indent size is comparable to the splat dimensions, thus allowing the inspection of inter-splat bonding in the indent area.

Splat separation was consistently found throughout the coarse coating. This can be seen in the spreading of the indent as the splats separate (coarse, upper left). Splat separation also suggests that no metallurgical bonds are formed despite the visible lack of oxide at the splat interfaces, hence allowing easy separation under the shear stresses imposed by the indenter. The low level of splat interaction is most likely caused by low particle velocities, possibly in connection with lower particle temperatures. The evidence for the insufficient velocity and temperature is indirect; however, observations reported in literature [2] support these conclusions. It was reported that cold spray (five to seven times higher particle velocity than APS) coatings exhibit a very low porosity (1.5% given in Ref. [2]) but have weakly bonded splats similar to our findings. For the coarse coating it can be deduced that, compared to the cold-spray coating in Ref. [2], the higher porosity indicates a low particle velocity, and the weak inter-splat bonding indicates a low particle temperature.

Separation is still visible for the medium coating (arrow on left corner of indent) but only pore-separated splats are affected. No visible separation is found for the mixed and the fine coatings where the indent crosses oxide zones without discontinuity. This suggests a good contact between the oxide scales of different splats, likely caused by higher particle velocities and temperatures. The clear separation of splats indicates re-melting of the metal and further post-impact oxidation during which the oxide layers of different splats grow together. The oxide itself is not likely to re-melt because the typical in-flight particle temperature (2340 °C [2]) of air plasma spray is insufficient (Cr_2O_3—$T_{melt} = 2435$ °C [28]).
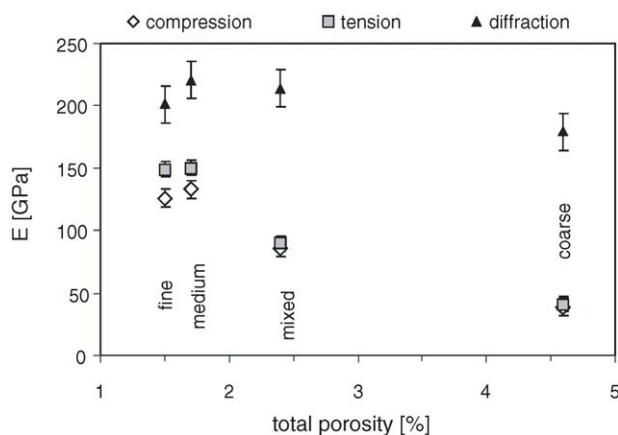
Fig. 8. Young's modulus as obtained by diffraction from tensile bending of the coatings attached to the substrate ((3 1 1) reflection) as well as from four point bending of delaminated coatings. The terms 'compression' and 'tension' refer to the stress at the coating outer surface (as opposed to the coating interface surface).
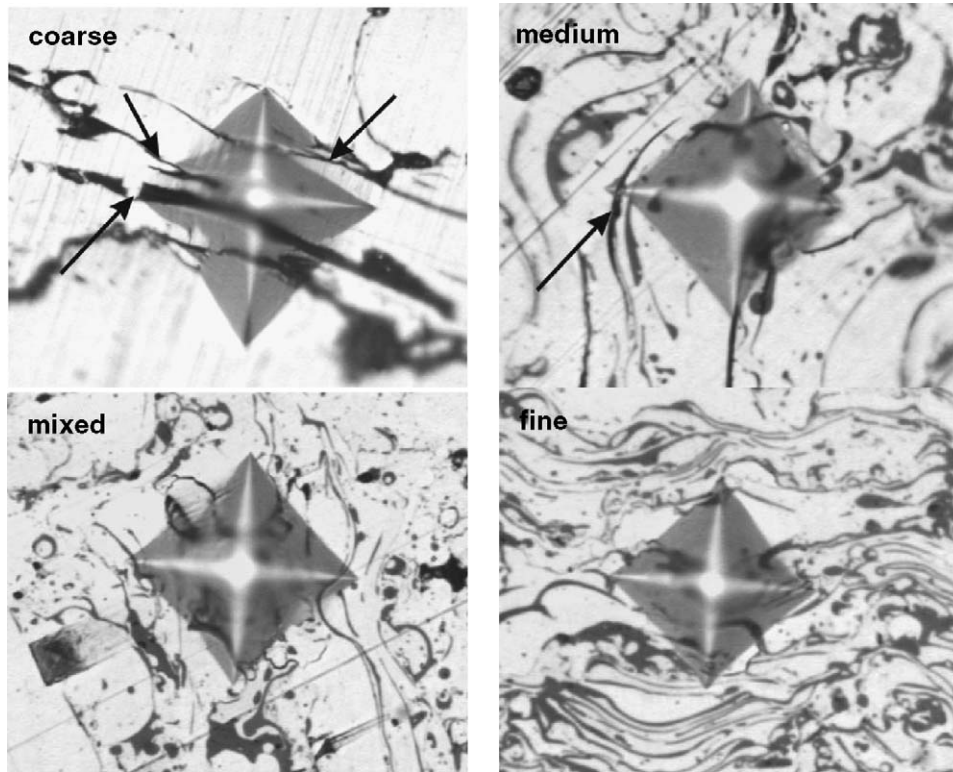
Fig. 9. Vickers indents (varying magnification) in the coating cross-section. Splat separation is indicated by arrows and by the apparent double and triple overlay of indenter images (coarse). See also the clear image of the indent for the fine coating.

The numerical results of the hardness tests are shown in Fig. 10. The effects of porosity and oxide content on the hardness are opposite, i.e. the hardness increases as the oxide content increases and the porosity decreases. The dispersed oxide particles perform the same way as ceramic reinforcements in a metal–ceramic composite; the yield stress and the hardness are

increased. Pores accommodate deformation without resistance, thus decreasing the hardness as the porosity increases. Large feed stock particles, due to their better volume to surface ratio, exhibit lower in-flight oxidation but the coatings show the largest porosity, both resulting in low hardness. The opposite is found for the fine coatings that have the smallest porosity and the highest oxide content, thus showing a significant increase in hardness. The hardness increase suggests a similarly substantial decrease in ductility, thus making smaller particle coatings less strain tolerant, i.e. less able to accommodate deformations of the substrate.

3.6. Residual stresses

The average residual stresses are shown in Fig. 11. The residual stresses are tensile as a result of thermal quenching stresses. The mismatch of the coefficients of thermal expansion (CTE) of substrate and coatings is very small [3], therefore the mismatch stresses are low. However, it should be noted that the rising Cr_2O_3 content gives rise to stresses between the IN625 metal phase and Cr_2O_3. Because of the lower CTE for chromia compared to IN625 (7.5×10^{-6} m/K versus 13.3×10^{-6} m/K [13,28]) the room temperature stresses in the metal phase become more tensile with higher oxide content. Also, the stresses decrease with increasing porosity and follow the dependence of Young's modulus on the porosity. This strongly suggests that, assuming comparable levels of thermal quenching strains in the splats, the residual stresses largely depend on Young's modulus which itself depends strongly on the
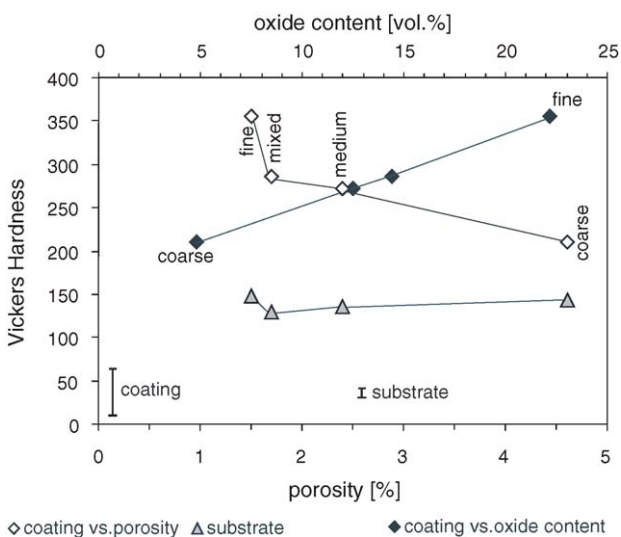
Fig. 10. Average hardness of IN625 plasma sprayed coatings. The coating hardness is plotted twice: the black symbols are plotted against the upper *x*-axis (oxide content) the empty symbols are plotted against the lower *x*-axis (porosity). The substrate hardness is provided for reference. The connecting lines serve as guide for the eye.
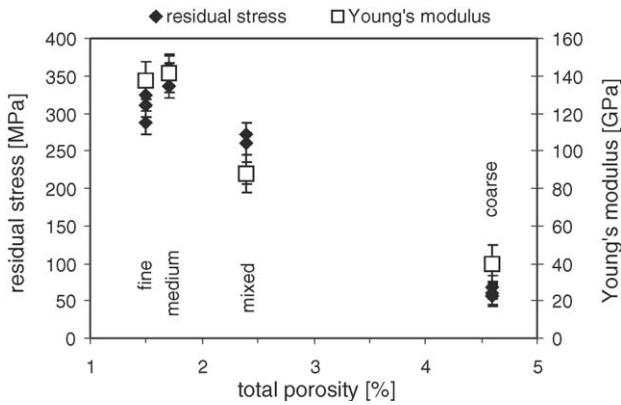
Fig. 11. Residual stresses (in-plane) in IN625 coatings. Also plotted is the average elastic modulus determined from detached coatings (right axis). Residual stress values are shown for three specimens for each particle size.

pore structure. However, stresses have a larger percent-decrease over the porosity than Young's modulus, thus indicating some degree of stress relaxation for large particle coatings. The low oxide content together with the highest porosity and the lowest hardness – mechanisms that lower the yield stress – provide evidence that the coarse coatings are affected the most by yielding during cooling.

3.7. Adhesion

The results of the adhesion tests are shown in Fig. 12. Results for NiCrAlY from the same test procedure are provided for reference.

The best adhesive strength is achieved by the mixed powder that contains all particle sizes (size range −200 to +5 μm). It should be noted that the same adhesive strength is found in NiCrAlY with a (−106 to +45 μm) particle size range. The results for the narrower particle size distributions–coarse, medium, and fine-suggest that neither very large nor very small particles produce high adhesion. The adhesive strength of the medium coating is comparable to that of the mixed coatings that have a much wider particle size distributing.
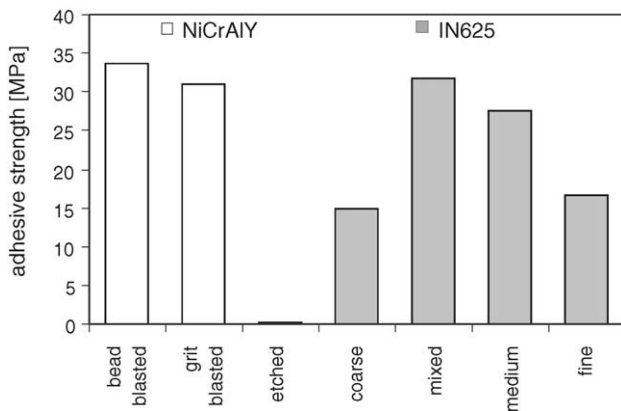
Fig. 12. Results of the adhesion pull tests on IN625 (all grit blasted substrates) and NiCrAlY coatings (grit/bead blasted and etched substrates). The uncertainty is approximately 6 MPa.

Sobolev et al. [19,20] conducted an analysis of a number of effects that influence coating adhesion. The oxide content and magnitude of the residual stresses were shown to be detrimental for adhesion. Both quantities are highest for the fine coatings that have the second lowest adhesion among the IN625 coatings. However, stresses are similarly high for mixed and medium coating, both with lower oxide fractions and with high adhesive strength. Furthermore, it was pointed out that the adhesion increases both with increasing particle velocity and with increasing thermal energy of the droplet. The poor inter-splat interaction found in the coarse coatings (Fig. 9, upper left) suggests that particle velocities were at the low end of the velocity spectrum of the spray process, therefore causing low coating adhesion. Also, low particle temperatures cannot be ruled out as contributing factor. Fine, medium, and mixed coatings have smaller porosities than the coarse coating and show little or no splat separation in hardness tests which leads to the conclusion that particle velocities were higher. This points indirectly to the oxide content, possibly as a solidified surface layer on the particles prior to impact, as a factor for low adhesion.

Another possible factor affecting adhesion is the combination of substrate surface feature size and splat size. Evidence for the existence of an optimal combination of surface peak spacing and splat size was presented in Refs. [18,29], where it was experimentally shown that adhesion increases proportionally to the average surface roughness but has a maximum for a certain ratio of splat size (which depends on the particle size) to peak spacing. In our work, neither the splat sizes nor the surface peak spacings were analyzed but it can be assumed that the splat sizes vary in a similar fashion to the particle sizes (factor 4 from fine to coarse), thus covering an equally large range of ratios of peak spacings (all substrates underwent the same grit blasting) to splat size. Although the findings shown in Fig. 12 are consistent with the results in Ref. [29] the evidence is only indirect.

4. Summary and conclusions

In this work, the effect of the particle size distribution on the microstructure and on the mechanical properties of plasma sprayed IN625 coatings was examined. The porosity increases with the particle size and for large particles is almost entirely comprised of surface connected pores. This is seemingly correlated with the poor bonding between splats for coarse particles, and is seen as an indication for comparatively low particle velocities and, possibly, low particle temperatures. Fine coatings have little porosity; the microstructure is mostly characterized by high fractions of Cr_2O_3 formed on the splat interfaces. Splat interaction is characterized by good cohesion which was interpreted as a result of post-impact oxidation. The oxide content increases strongly with the increasing surface to volume ratio of smaller particles.

The investigation of the elastic properties showed that both strain response and Young's modulus decrease with increasing porosity. Compared to the small influence of the oxide content, this behavior was interpreted as mostly the effect of the rising surface connected porosity. Connections between pores, e.g. through poorly bonded splats, is seen as an effective increase

of the average pore aspect ratio. High porosity and weak inter-splat interaction in coarse coatings is also likely to cause the deformation to be partially inelastic, thus further reducing both the modulus and the elastic response.

The hardness tests reveal that the behavior in plastic deformation is controlled both by the oxide content and the porosity. Small feed stock particle coatings have low porosity and high oxide content which together account for steep increase in hardness for the fine coating.

For the residual stresses it was found that the stress level declines strongly as the particle size and porosity increase. The quenching strains are assumed to be equal, thus leading to the conclusion that the Young's modulus largely controls the residual stresses in the coatings. Inelastic processes are again likely to contribute to the low stress level in coarse coatings.

The best adhesive strength was found for intermediate particle sizes. Indirect evidence indicates that adhesion is limited both by insufficient particle velocities and thermal energies for coarse particles. The limitation for fine particles is likely caused by the high oxide content. The ratio of substrate surface peak spacing to splat size was also discussed as an influence on adhesion. However, due to different levels of stress, oxide content, and particle velocities no clear conclusion can be drawn on the magnitude of this effect.

References

[1] L. Pawlowski, The Science and Engineering of Thermal Spray Coatings, Wiley & Sons, Chichester, 1995.

[2] S. Sampath, et al., Mater. Sci. Eng. A 364 (2004) 216–231.

[3] O. Kesler, et al., Mater. Sci. Eng. A 257 (2) (1998) 215–224.

[4] A.J. Allen, et al., Acta Mater. 49 (9) (2001) 1661–1675.

[5] I. Sevostianov, M. Kachanov, Mater. Sci. Eng. A 297 (2001) 235–243.

[6] J. Matejicek, et al., in: C.C. Berndt (Ed.), Thermal Spray: Surface Engineering via Applied Research, ASM, Materials Park, OH, 2000, ISBN 0-87170-680-6, pp. 351–354.

[7] T. Gnäupel-Herold, et al., in: E.E. Gdoutos (Ed.), Recent Advances in Experimental Mechanics, Kluwer Academic Publishers, Dordrecht, 2002, pp. 507–514.

[8] F. Kroupa, J. Dubský, Scripta Mater. 40 (11) (1999) 1249.

[9] S. Leigh, C.C. Berndt, Acta Mater. 47 (5) (1999) 1575–1586.

[10] R. McPherson, Surf. Coat. Technol. 39–40 (1–3) (1989) 173.

[11] J.R. Willis, Adv. Appl. Mech. 21 (1981) 1–78.

[12] J. Matejicek, S. Sampath, T. Gnaeupel-Herold, H.J. Prask, Appl. Phys. A 74 (Suppl. 8) (2002) S1692–S1694.

[13] J. Matejicek, et al., Acta Mater. 47 (2) (1999) 607–617.

[14] Y.C. Tsui, et al., Acta Met. Mater. 42 (8) (1994) 2837–2844.

[15] T.W. Clyne, S.C. Gill, J. Thermal Spray Technol. 5 (4) (1996) 401.

[16] S. Kuroda, T. Fukushima, S. Kitahara, in: C.C. Berndt (Ed.), Proceedings of the International Thermal Spray Conference, ASM, Materials Park, 1992, pp. 903–909.

[17] J. Matějíček, S. Sampath, H. Herman, in: C. Coddet (Ed.), Proceedings of the 15th International Thermal Spray Conference, ASM, Materials Park, 1998, pp. 419–424.

[18] M.F. Bahbou, et al., J. Thermal Spray Technol. 13 (4) (2004) 508–514.

[19] V.V. Sobolev, et al., Int. Mater. Rev. 42 (3) (1997) 117–136.

[20] V.V. Sobolev, et al., J. Thermal Spray Technol. 9 (1) (2000) 100–106.

[21] C.J. Li, W.Y. Li, Surf. Coat. Technol. 162 (1) (2003) 31–41.

[22] T. Gnaeupel-Herold, H.J. Prask, R.J. Fields, T.J. Foecke, Z.C. Xia, U. Lienert, Mater. Sci. Eng. A 366 (2004) 104–113.

[23] A.A. Boudi, M. Hashmi, B.S. Yilbas, J. Mater. Process. Technol. 155–156 (2004) 2051–2055.

[24] ASTM Designation C 633–79, Standard Test Method for Adhesion or Cohesive Strength of Flame Spayed Coatings, 1979.

[25] T. Gnäupel-Herold, P.C. Brand, H.J. Prask, J. Appl. Cryst. 31 (1998) 929–935.

[26] F. Bollenrath, V. Hauk, E.H. Müller, Z. Metallkd. 58 (1967) 76–82.

[27] T. Mura, Micromechanis of Defects in Solids, Martinus Nijhoff Publishers, Dordrecht Boston Lancaster, 1987 (Chapter 3).

[28] J. Dubsky, H.J. Prask, J. Matejicek, T. Gnaeupel-Herold, Appl. Phys. A 74 (Suppl. 8) (2002) S1115–S1117.

[29] D.T. Gawne, B.J. Griffiths, G. Dong, Trans. Inst. Met. Finish. 75 (Part 6) (1997) 205–207.